



Synthesis and photophysical properties of tetraphenylethylene derivatives as luminescent downshifting materials for organic photovoltaic applications

Hélio Lopes Barros, Maria Alexandra Esteves, Maria João Brites*

National Laboratory of Energy and Geology (LNEG), Renewable Energies and Energy Efficiency Unit. (UEREE), Estrada do Paço do Lumiar, 22, 1649-038, Lisboa, Portugal

ARTICLE INFO

Keywords:

Organic solar cells
Luminescent dyes
UV filters
Luminescent down-shifting
Intramolecular charge-transfer

ABSTRACT

Luminescent Down-Shifting (LDS) is an optical approach applied in several photovoltaic (PV) technologies in which high energy solar radiation is converted to a wavelength region where the response of the photovoltaic devices is better. The use of LDS layers on organic photovoltaics (OPV) could serve two purposes: to prevent cell degradation by filtering the incident ultraviolet (UV) radiation and to improve the spectral response of PV cells at short-wavelength. This work reports, the design and synthesis of a series of tetraphenylethylene (TPE) derivatives based on TPE-A or A- π -TPE- π -A molecular structure featuring various electron-acceptor (A) groups. The photophysical properties of the new LDS compounds were systematically studied in 1,4-dioxane solution and film (Zeonex) by UV-visible absorption and fluorescence spectroscopy, and electrochemical properties studied by cyclic voltammetry. Thermal stability of the new LDS compounds was evaluated by Thermogravimetric analysis (TGA). Theoretical computational studies provided evidence of existence of intramolecular charge-transfer (ICT) between frontier orbitals of donor and acceptor moieties. The good photophysical and thermal properties of the synthesized TPE derivatives, associated with high molar absorption coefficients in UV spectrum and emission maximum in the range of 476–531 nm, make them promising candidates for LDS layers in OPV application.

1. Introduction

Luminescent Down-Shifting (LDS) is an optical approach applied in several photovoltaic (PV) technologies to improve the spectral match between solar cells and the distribution of sunlight (AM 1.5 G). The LDS layer consists of a polymer sheet (e.g poly (methyl methacrylate PMMA, ethylene vinyl acetate EVA polymer) with luminescent molecules embedded in it, which can absorb the short wavelength (λ) photons, where the PV cell responds poorly ($\lambda < 400$ nm) and re-emit photons in the visible spectrum, where its spectral response is much greater.

The use of LDS layers positioned on top of the PV cell (Scheme 1) could serve two purposes: to prevent cell degradation by filtering the incident ultraviolet (UV) radiation and to improve the spectral response of PV cells at short-wavelength [1]. So far, the majority of studies have focused on the effects of LDS in the external quantum efficiency (EQE) of solar cells [2–5]. Although the stability issue is a major obstacle for the commercialization of the emerging PV technologies, such as organic photovoltaic (OPV) and perovskite (PSC) cells, the potential for

efficiency and stability enhancements via LDS layer on these PV materials and devices were investigated only in a few number of published studies [1,6,7]. It's known that some components of OPV, namely the active layer, are susceptible to photodegradation, due to the combined effect of the UV component of solar radiation and oxygen from the ambient air [8–10]. Kettle et al [1]. and Fernandes et al. [7,11] have reported promising results demonstrating the proof of concept of improvement of both the lifetime and efficiency of OPV cells by applying LDS layers based on a lanthanide-based metal complex [1] or a mixing of two luminescent materials forming multi-dye blends, respectively [7, 11].

Over the years, a large number of luminescent materials, such as organic dyes [7], quantum dots [12,13] and rare-earth ion complexes [14,15] have been investigated for their use as LDS layers. In particular, organic dyes have been highlighted for presenting high absorption coefficient, good Luminescent Quantum Yield (LQY), large Stokes shift i. e, good shift between absorption and emission bands, and good solubility in polymeric matrix [11,16]. However, most of the organic dyes already

* Corresponding author.

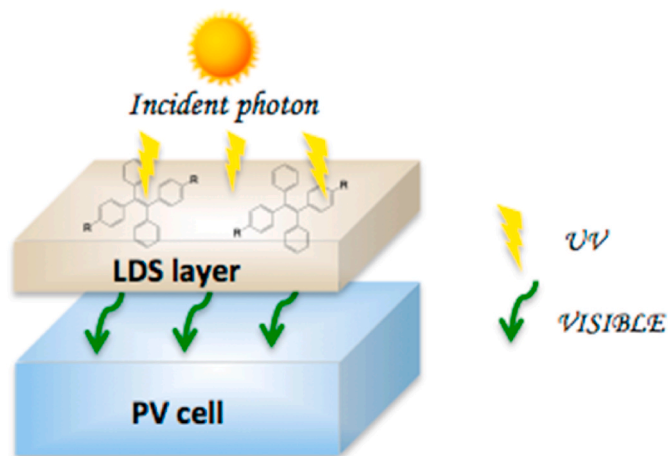
E-mail addresses: helio.barros@lneg.pt (H.L. Barros), alexandra.esteves@lneg.pt (M.A. Esteves), mjoao.brites@lneg.pt (M.J. Brites).

<https://doi.org/10.1016/j.dyepig.2021.109724>

Received 5 March 2021; Received in revised form 21 July 2021; Accepted 14 August 2021

Available online 15 August 2021

0143-7208/© 2021 Elsevier Ltd. All rights reserved.



Scheme 1. Schematic of the down-shifting mechanism of a PV cell with a LDS layer on top.

tested for LDS [7,17] were designed for other applications (e.g. BASF Lumogen dyes [18], showing narrow absorption bands or spectral mismatch between their emission light and the spectral response of solar cells.

To improve the efficiency and stability of OPV, an ideal LDS material should exhibit optical properties, such as wide absorption of UV component of solar radiation, high absorption coefficient, high Luminescence Quantum Yield (LQY), high transmittance, large Stokes Shift and long-term photo and thermal stability [7].

The tetraphenylethene (TPE) molecule, exhibiting Aggregation-induced Enhanced Emission (AEE) characteristics, is a versatile building block, for the development of luminescent materials with efficient solid-state emissions [19]. TPE derivatives have been reported as sensitizers for dye-sensitized solar cells [20,21], however up to date, their use as LDS materials are scarce and limited to Cadmium Tellurium (CdTe) PV. Li et al. [5] reported the applications of some TPE dyes for CdTe solar cell, with an increase in the output short circuit current density (J_{sc}) of 5.69% for a small cell and 8.88% for a large panel. These fluorophores proved to exhibit superior capabilities of LDS when compared with BASF Lumogen dyes, violet (V570) and yellow (Y083) commercially available [22].

One way to fine-tuned optical properties of organic dyes is achieved by manipulating the charge densities of the donor and/or the acceptor, allowing to reach various Intramolecular Charge transfer (ICT) rates, from the donor to the acceptor upon molecular excitation. A high ICT rate will result in a large change in the transition dipole moment of the molecule, and consequently induces a large Stokes shift.

In this study, we report the synthesis of luminescent down shifter tetraphenylethene (TPE) derivatives designed for enhancing efficiency and stability of OPV cells. Donor-Acceptor TPE derivatives were synthesized using TPE core as donor and as an AEE functional group, linked to one or two acceptors (A), with different electron withdrawing strength, with the aim to establish a structure-properties relationship of emission behavior. The electron-acceptor groups selected were nitro, cyano, di-cyano, cyanoacetic acid, or hexylcyanoacetate. The photo-physical and electrochemical properties of TPE-A and A- π -TPE- π -A luminescent dyes were investigated, and the obtained results make them promising LDS materials for OPV and PSC applications.

2. Experimental Section

2.1. Materials and methods

All reagents and solvents used in the synthesis, purification, photo-physical and electrochemical studies of the TPE derivatives were

purchased from TCI and were used without further purification, except for tetrahydrofuran (THF) and acetonitrile which were previously dried by standard procedures [23]. Zeonex and PMMA (polymethyl methacrylate) polymers were purchased from Aldrich. Hexyl-2-cyanoacetate and $\text{Pd}(\text{PPh}_3)_2\text{Cl}_2$ were prepared by previously described procedures [24,25]. Spectroscopic solvents (Eurisotop® and Cambridge isotope Laboratories, Inc®) were used to prepare samples for spectroscopic characterization. ^1H and ^{13}C nuclear magnetic resonance (NMR) spectra were obtained with a BRUKER, AVANCE 400 MHz Ultra Shield spectrometer at the Faculty of Sciences of Lisbon University. The chemical shifts are reported in δ (ppm) and coupling constants in Hertz (Hz). Fourier-transform infrared spectroscopy (FTIR) spectra were obtained in KBr pellet and NaCl cells using an Elmer Spectrum BX v5.3.1 spectrometer. High resolution mass spectra (HR-MS) with electron spray ionization (ESI) were performed on a microTOF-Focus mass spectrometer at CACTI of Vigo University. Melting points were determined in a Reichert Thermovar apparatus and were uncorrected. Thin layer chromatography (TLC) was performed on silica gel 60 F254 plates with 0.2 mm layer thickness from Merck, and column chromatography (CC) was carried out with Merck Si gel 60 (230–400 mesh). The synthesized products were observed under UV light at 254, 365 or 395 nm. Absorption spectra were recorded in quartz cuvettes using a Shimadzu UV-3101PC UV-Vis-NIR spectrophotometer. The fluorescence measurements were obtained using a Horiba Jobin Yvon Fluorolog 3 spectrometer. The excitation wavelength beam was adjusted to the maximum absorbance of the derivatives in films and the maximum wavelength of the reference standard for measurement in solution of 1, 4-dioxane. The photophysical experiments were all performed at room temperature and in a concentration range from 10^{-4} to 10^{-5} M. The Zeonex-based films were prepared by mixing 1 mg of synthesized dye and 100 mg of polymer (Zeonex) in 1 mL of toluene. The mixture was stirred at room temperature overnight or until the polymer was completely dissolved. The dye-polymer mixture was poured into a quartz piece (4×1 cm) by drop-casting using a Pasteur pipette. The solvent was evaporated under room temperature and further dried in a desiccator under vacuum for 48 h. The PMMA-based films were prepared by solution of 25 mg of PMMA in 1 mL of toluene with different concentration of dye D8 and D11 (0.03, 0.05, 0.11, 0.34 and 0.57% wt). The mixture solution was sonicated in an ultrasound bath for 20 min and deposited into a quartz piece (4×1 cm) by spin-coating at 100 rpm for 60s using a LAURELL® – technologies corporation, model WS-650HZ-23NPPB/OND. The solvent was evaporated under room temperature and further dried in a desiccator under vacuum for 24 h.

2.2. Synthetic procedures

2.2.1. 2,6-Difluoro-4-(1,2,2-triphenylvinyl)benzaldehyde (6)

A mixture of 2-bromo-1,1,2-triphenylethylene 5 (168 mg, 0.5 mmol), $\text{Pd}(\text{PPh}_3)_2\text{Cl}_2$ (30 mg, 0.05 mmol) and K_2CO_3 (690 mg, 5 mmol) in 20 mL of THF/H₂O (4:1) was stirred in reflux at 85 °C under N₂. The coupling reagent, 3,5-difluoro-4-formylphenyl boronic acid (111 mg, 0.6 mmol), was dissolved in THF and added to the reaction mixture after 30 min using a syringe. The reaction was followed by thin layer chromatography using a mixture of hexane/ethyl acetate (5:1) as eluent. As soon as the reaction was completed (24 h), the reaction mixture was filtered in vacuum over Celite to remove metal catalyst. After that, 30 mL of water was added and extracted twice with 15 mL of dichloromethane. The organic phase was dried over anhydrous magnesium sulfate and the solvent evaporated under reduced pressure. The product was purified by column chromatography on silica gel, using dichloromethane/hexane (1/2) as eluent. The product was obtained as a light yellow solid (163 mg, $\eta = 82\%$). m. p.: 121–123 °C; FTIR (KBr): 3053, 3020 (C–H aromatic), 2865, 2774 (C–H aldehyde) 1700, 1625 (C=O carbonyl), 1560 (C=C aromatic ring), 1443, 1420, 1409, 1208 (C–F), 870, 761 (C–H aromatic), 698 cm^{-1} (C=C alkene). ^1H NMR (400 MHz, CD_3COCD_3): δ 6.76 (2H, d, $J = 8$ Hz), 7.03–7.23 (15H, m), 10.18 (1H, s)

ppm. ^{13}C NMR (100 MHz, CD_3COCD_3): δ 113.0, 115.7, 115.9, 128.0, 128.1, 128.4, 128.6, 129 (2C), 131.7 (2C), 131.9, 138.9, 142.7, 143.3, 143.4, 145.4, 153.9, 161.9, 164.5, 184.3 ppm. HRMS (ESI) $[\text{M}+\text{H}]^+$: m/z calcd. ($\text{C}_{27}\text{H}_{18}\text{F}_2\text{O}$) 397.1405; found 397.1391.

2.2.2. Hexyl 2-cyano-3-(2,6-difluoro-4-(1,2,2-triphenylvinyl)phenyl)acrylate (D6)

A mixture of 2,6-difluoro-4-(1,2,2-triphenylvinyl)benzaldehyde (6) (120 mg, 0.302 mmol), hexyl-2-cyanoacetate (77 mg, 0.453 mmol) and ammonium acetate (9.4 mg, 0.121 mmol) in 10 mL of glacial acetic acid was stirred at 120 °C in reflux under N_2 for 3 h. The reaction was followed by thin layer chromatography using a mixture of dichloromethane/hexane (1/2) as eluent. After cooling to room temperature, a saturated sodium bicarbonate solution was added and the resulting mixture was extracted by ethyl acetate. The combined organic phases were dried with anhydrous magnesium sulfate and concentrated in vacuo. Purification was done by column chromatography on silica gel, using dichloromethane/hexane (1/2 then 1/1) as eluent. The product was obtained as a thick yellow oil (137 mg, η = 83%). FTIR (NaCl): 3079, 3056, 3025 (C–H aromatic), 2957, 2930, 2859 (C–H alkyl) 1734, 1701, 1626 (C=O), 1560, 1492, 1444 (C=C aromatic ring), 1258, 1215, 1200, 1098, 1027 (C–F, C–O), 762, 699 cm^{-1} (C=C alkene, C–H aromatic); ^1H NMR (400 MHz, CD_3COCD_3): δ 0.89 (3H, s), 1.28–1.44 (6H, m), 1.74 (2H, t, J = 4 Hz), 4.32 (2H, brs, 6.83 (2H, d, J = 12 Hz), 7.06–7.23 (15H, m), 8.18 (1H, s) ppm. ^{13}C NMR (100 MHz, CD_3COCD_3): δ 14.2, 23.2, 26.1, 29.1, 32.1, 67.6, 109.3, 112.0, 114.3, 115.3, 115.6, 128.0, 128.1, 128.4, 128.6 (2C), 129.0 (2C), 129.1 (2C), 131.7, (2C), 131.9 (2C), 138.7 (2C), 139.0, 143.0, 143.3, 143.4, 145.3, 148.8, 151.9, 159.4 (2C), 161.9 ppm. HRMS (ESI) $[\text{M}+\text{H}]^+$: m/z calcd. ($\text{C}_{36}\text{H}_{31}\text{F}_2\text{N}_2\text{O}_2$) 548.2356; found 548.2401.

2.2.3. 2-(2,6-Difluoro-4-(1,2,2 triphenylvinyl)benzylidene)malononitrile (D7)

Compound D7 was synthesized by the procedure used for compound D6. The method was used with 2,6-difluoro-4-(1,2,2-triphenylvinyl)benzaldehyde (6) (150 mg, 0.378 mmol) and malonitrile (36 μL , 0.567 mmol). Purification was performed by silica column chromatography using dichloromethane/hexane (1/1) as eluent, and the product was obtained as a yellow foam (140 mg, η = 83%). m. p.: 155–157 °C; FTIR (KBr): 3056, 3019 (C–H aromatic), 2922 (C–H alkyl), 1626, 1598, 1560, 1421 (C=C aromatic ring), 1026, 1272 (C–F), 697 cm^{-1} (C=C alkene, C–H aromatic) ^1H NMR (400 MHz, CD_3COCD_3): δ 6.87 (2H, d, J = 12 Hz), 7.06–7.24 (15H, m), 8.21 (1H, s) ppm. ^{13}C NMR (100 MHz, CD_3COCD_3): δ 90.4, 108.8, 112.4, 114.1, 115.5, 115.8, 128.1, 128.2, 128.5, 128.6 (2C), 129.0 (2C), 129.1 (2C), 131.7 (4C), 131.9 (2C), 138.8, 142.7, 143.3, 143.4, 145.7, 149.5, 153.4, 159.3, 161.8. Ppm. HRMS (ESI) $[\text{M}]^+$: m/z calcd. ($\text{C}_{30}\text{H}_{18}\text{F}_2\text{N}_2$) 444.1438; found 444.1463.

2.2.4. 2-Cyano-3-(2,6-difluoro-4-(1,2,2-triphenylvinyl)phenyl)acrylic acid (D8)

Compound D8 was synthesized by the procedure used for compound D6. The method was used with 2,6-difluoro-4-(1,2,2-triphenylvinyl)benzaldehyde (6) (150 mg, 0.378 mmol) and 2-cyanoacetic acid (48 mg, 0.567 mmol). Purification was performed by silica column chromatography, using ethyl acetate/methanol (9/1) as eluent and the product was obtained as an orange foam (136 mg, η = 77%). m. p.: 224–226 °C; FTIR (KBr): 3421 (O–H carboxylic acid), 3056, 3023 (C–H aromatic), 1628 (C=O), 1597, 1560, 1491, 1419, 1389 (C=C aromatic ring), 1026 (C–O, C–F), 698 cm^{-1} (C=C alkene, C–H aromatic); ^1H NMR (400 MHz, CD_3COCD_3): δ 6.65 (2H, d, J = 12 Hz), 7.05–7.16 (15H, m), 8.04 (1H, s) ppm. ^{13}C NMR (100 MHz, CD_3COCD_3): δ 65.1, 109.6, 114.0, 114.2, 115.5, 126.9, 127.0, 127.3, 127.6 (2C), 127.9 (2C), 128.0 (2C), 130.7 (2C), 130.8 (2C), 130.9 (2C), 138.1138.5, 142.0, 142.4, 142.7, 143.7, 148.7, 158.2, 160.7, 166.0 ppm. HRMS (ESI) $[\text{M}+\text{H}]^+$: m/z calcd. ($\text{C}_{30}\text{H}_{19}\text{F}_2\text{NO}_2$) 464.1462; found 464.1469.

2.2.5. 1,2-bis(4-Bromophenyl)-1,2-diphenylethene (8)

TiCl_4 1 M in toluene (4.21 mL, 4.21 mmol) was added to a mixture of 4-bromobenzophenone (7) (1 g, 3.83 mmol) and zinc dust (0.50 g, 7.66 mmol) in dry THF (10 mL) in a round bottom flask under nitrogen atmosphere. The mixture was stirred at reflux temperature until complete consumption of 7 (20 h) as judged by TLC (dichloromethane/hexane, 1/3). The mixture was quenched with 10% K_2CO_3 solution and filtered. The filtrate was extracted three times with THF and the resulting organic layer was washed with brine and dried over anhydrous magnesium sulfate. After solvent evaporation, the crude product was purified by silica column chromatography using dichloromethane/hexane (1/3) as eluent. A mixture (1/1) of the *cis* and *trans* isomers of the product was obtained as a white solid after recrystallization from dichloromethane/methanol (0.636 g, η = 68%). m. p.: 183–185 °C; FTIR (KBr): 3074, 3055, 3020 (C–H aromatic), 1487, 1442, 1409, 1391 (C=C aromatic), 1071, 1010, 805, 758, 696 cm^{-1} (C=C alkene, C–H aromatic, C–Br). ^1H NMR (400 MHz, CD_3COCD_3): δ 6.98 (4H, t, J = 8 Hz), 7.03–7.07 (4H, m), 7.13–7.18 (6H, m), 7.31 (2H, d, J = 8 Hz), 7.36 (2H, d, J = 8 Hz) ppm. ^{13}C NMR (100 MHz, CD_3COCD_3): δ 121.0, 121.2, 127.7, 127.8, 128.7, 128.9, 131.7, 131.8, 131.9, 133.8, 133.9, 141.4 (2C), 143.5, 143.6, 143.7, 143.8 ppm. HRMS (ESI) $[\text{M}+\text{H}]^+$: m/z calcd. ($\text{C}_{26}\text{H}_{18}\text{Br}_2$) 490.9834; found 490.9852.

2.2.6. 4',4'''-(1,2-diphenylethene-1,2-diyl)bis(3,5-difluoro-[1,1'-biphenyl]-4-carbaldehyde) (9)

Compound 9 was synthesized by the procedure used for compound 6. The method was used with 1,2-bis(4-bromophenyl)-1,2-diphenylethene (8) (147 mg, 0.3 mmol), 3,5-difluoro-4-formylphenyl boronic acid (204 mg, 1.1 mmol), $\text{Pd}(\text{PPh}_3)_2\text{Cl}_2$ (42 mg, 0.06 mmol) and K_2CO_3 (0.83 g, 6.0 mmol). Purification was performed by silica column chromatography using ethyl acetate/hexane (1/3) as eluent, to give a mixture (1:1.2) of the *cis* and *trans* isomers of the product as a yellow solid (121 mg, η = 66%). m. p.: 92–94 °C; FTIR (KBr): 3024 (C–H aromatic), 2867 (C–H aldehyde) 1701, 1626 (C=O), 1570, 1550, 1432, 1410, 1396 (C=C aromatic), 1200, 1183, 1039 (C–F), 894, 701 cm^{-1} (C–H aromatic, C–H alkene); ^1H NMR (400 MHz, CD_3COCD_3): δ 7.10–7.20 (12H, m), 7.24 (2H, d, J = 8 Hz), 7.45 (2H, d, J = 8 Hz), 7.46 (2H, d, J = 8 Hz), 7.63 (4H, t, J = 8 Hz), 10.28 (1H, s), 10.30 (1H, s) ppm. ^{13}C NMR (100 MHz, CD_3COCD_3): δ 110.9, 111.2, 113.4, 127.3, 127.5, 127.7, 127.9, 128.8, 128.9, 131.9, 132.0, 132.8, 132.9, 135.9, 136.0, 142.0, 144.0, 146.1, 149.4, 162.8, 162.9, 165.5, 184.4 ppm. HRMS (ESI) $[\text{M}+\text{H}]^+$: m/z calcd. ($\text{C}_{40}\text{H}_{24}\text{F}_4\text{O}_2$) 613.1791; found 613.1780.

2.2.7. Di-hexyl 3,3'-((1,2-diphenylethene-1,2-diyl)bis(3,5-difluoro-[1,1'-biphenyl]-4',4'-diyl)) (2E,2'E)-bis(2-cyanoacrylate) (D9)

Compound D9 was synthesized by the procedure used for compound D6. The method was used with 4',4'''-(1,2-diphenylethene-1,2-diyl)bis(3,5-difluorobiphenyl-4-carbaldehyde) (9) (107 mg, 0.175 mmol) and hexyl-2-cyanoacetate (89 mg, 0.525 mmol). Purification was performed by silica column chromatography using dichloromethane/hexane (1/1) as eluent. A mixture of the *cis* and *trans* isomers of the product was obtained as a thick yellow oil (120 mg, η = 75%). FTIR (NaCl): 3056 (C–H aromatic), 2957, 2932, 2860 (C–H alkyl), 1732, 1629 (C=O), 1433, 1261 (C=C aromatic), 1222, 1100, 1028 (C–O, C–F), 701 cm^{-1} (C–H aromatic, C=C alkene); ^1H NMR (400 MHz, CD_3COCD_3): δ 0.89 (6H, s), 1.26–1.46 (12H, m), 1.77 (4H, brs), 4.34 (4H, s), 7.11–7.26 (14H, m), 7.54 (4H, d, J = 8 Hz), 7.66 (4H, t, J = 8 Hz), 8.30 (2H, s) ppm. ^{13}C NMR (100 MHz, CD_3COCD_3): δ 14.3, 23.3, 26.2, 29.2, 32.2, 67.7, 110.0110.7, 111.0, 112.4, 114.5, 127.3, 127.4, 127.8, 128.0, 128.8, 129.0, 132.0, 132.1, 132.9 (2C), 136.2, 142.1, 144.1, 144.2143.2, 146.0, 146.1, 148.0, 160.4, 162.0, 162.9 ppm. HRMS (ESI) $[\text{M}+\text{H}]^+$: m/z calcd. ($\text{C}_{58}\text{H}_{50}\text{F}_4\text{N}_2\text{O}_4$) 915.3740; found 915.3778.

2.2.8. (2-(4-Nitrophenyl)ethene-1,1,2-triyl)tribenzene (D10)

Compound D10 was synthesized by the procedure used for compound 6. The method was used with 2-bromo-1,1,2-triphenylethylene

(250 mg, 0.746 mmol), 4-nitrophenyl boronic acid (149 mg, 0.895 mmol), Pd(PPh₃)₂Cl₂ (52.0 mg, 0.0746 mmol) and K₂CO₃ (1.03 mg, 7.46 mmol). Purification was performed by silica column chromatography using ethyl acetate/hexane (1/5) as eluent, and the product was obtained as a yellow solid (211 mg, η = 75%). m. p.: 148–149 °C; FTIR (KBr): 3053 (C–H aromatic), 1590 1512 (N–O), 1491, 1345 (C=C aromatic), 748, 699 cm⁻¹ (C–H aromatic, C=C alkene); ¹H NMR (400 MHz, CD₃COCD₃) δ 8.02 (2H, d, J = 7.8 Hz), 7.31 (2H, d, J = 7.5 Hz), 7.24–6.94 (15H, m) ppm. ¹³C NMR (100 MHz, CD₃COCD₃) δ 151.0, 146.1, 143.7, 142.9, 142.8, 142.6, 139.1, 132.1, 131.0, 130.9, 128.0, 128.0, 127.8, 127.2, 127.0, 122.8 ppm. HRMS (ESI) [M+H]⁺: m/z calcd. (C₂₆H₁₉NO₂) 378.1494; found 387.1493.

2.2.9. 4-(1,2-Triphenylvinyl)benzonitrile (D11)

Compound D11 was synthesized by the procedure used for compound 6. The method was used with 2-bromo-1,1,2-triphenylethylene (200 mg, 0.597 mmol), 4-cyanophenyl boronic acid (149 mg, 0.895 mmol), Pd(PPh₃)₂Cl₂ (42 mg, 0.060 mmol) and K₂CO₃ (825 mg, 5.970 mmol). Purification was performed by silica column chromatography using ethyl acetate/hexane (1/5) as eluent, and obtaining a white product (151 mg, η = 71%). m. p.: 171–173 °C; FTIR (KBr): 3051 (C–H aromatic), 2228 (CN nitrile), 1602, 1489, 1442, 1074 (C=C aromatic), 826, 744, 630, 596 cm⁻¹ (C=C alkene, C–H aromatic); ¹H NMR (400 MHz, CD₃COCD₃) δ 7.54 (2H, d, J = 8.1 Hz), 7.24 (2H, d, J = 8.1 Hz), 7.17 (9H, td, J = 6.5, 3.1 Hz), 7.06 (6H, dd, J = 6.6, 2.8 Hz) ppm. ¹³C NMR (100 MHz, CD₃COCD₃) δ 148.8, 143.2, 143.0, 142.9, 142.7, 139.5, 132.0, 131.5, 131.0, 130.9, 128.0, 128.0, 127.7, 127.0, 126.9, 118.4, 109.8 ppm. HRMS (ESI) [M+H]⁺: m/z calcd. (C₂₇H₁₉N) 358.1596; found 358.1598.

2.2.10. 1,2-bis(4'-Nitro-[1,1'-biphenyl]-4-yl)-1,2-diphenylethylene (D12)

Compound D12 was synthesized by the procedure used for compound 6. The method used 1,2-bis(4-bromophenyl)-1,2-diphenylethylene (8) (155 mg, 0.316 mmol), nitrophenyl boronic acid (127 mg, 0.759 mmol), Pd(PPh₃)₂Cl₂ (45 mg, 0.064 mmol) and K₂CO₃ (873 mg, 6.32 mmol). Purification was performed by silica column chromatography using ethyl acetate/hexane (1/5) as eluent, to give a mixture (1:3) of the *cis* and *trans* isomers of the product as a yellow solid (82 mg, η = 45%). m. p.: 254–256 °C; FTIR (KBr): 3024 (C–H aromatic), 1594, 1509 (N–O), 1342, 1108 (C=C aromatic), 805, 698 cm⁻¹ (C–H aromatic, C=C alkene); ¹H NMR (400 MHz, CDCl₃) δ 8.58 (1H, d, J = 6.8 Hz), 8.47 (3H, d), 8.28 (1H, d, J = 7.2 Hz), 8.10 (3H, d, J = 7.5 Hz), 7.81 (3H, t, J = 8.6 Hz), 7.38 (10H, dt, J = 28.6, 13.3 Hz) ppm. ¹³C NMR (100 MHz, CD₃COCD₃) δ 141.8 (3C), 141.7, 139.8, 139.2138.0, 135.7, 131.5, 131.4, 127.0 (2C) 126.2, 126.1, 123.1, 122.8, 122.7, 122.3, 121.8, 121.7, 121.6, 121.4, 119.2, 118.9 ppm. HRMS (ESI) [M+H]⁺: m/z calcd. (C₃₈H₂₆N₂O₄) 575.1971; found 575.1953.

2.3. Thermal analysis

Thermogravimetric analysis (TGA) and Differential Scanning Calorimetry (DSC) were carried on a SETSYS Evolution 1750/Simultaneous TGA DSC Thermal Analyzer (Setaram) under nitrogen atmosphere with gas flow of 20 mL min⁻¹. The sample with initial mass ranged from 3.369 to 12.281 mg was analyzed in a platinum crucible with temperature ranged from 20 to 600 °C and heating rate of 10 °C.min⁻¹.

2.4. Electrochemical properties

Cyclic voltammetry (CV) was performed on a potentiostat/galvanostat Gamry Instrument reference 600. The electrochemical cell was configured to work with three electrodes, a platinum disk, platinum wire and Ag/AgCl (3 M KCl solution) as working, counter and reference electrodes, respectively. The experiment was carried out at room temperature and scan rate of 50 mV/s. The supporting electrolyte was a solution of 0.1 M tetrabutylammonium hexafluorophosphate (TBAPF₆)

in dry acetonitrile, with concentration of dyes fixed at 2.5×10^{-3} M. The potential was calibrated against ferrocene/ferrocenium couple (Fc/Fc⁺). The HOMO energy level was calculated from the equation: E (HOMO) = -(E_{ox}^{onset} + 4.8) eV, where E_{ox}^{onset} is the onset oxidation potential versus Ag/Ag⁺ [26,27].

2.5. Quantum chemical calculations

Theoretical calculations were performed with Density Functional Theory (DFT) using the Gaussian 03 Package [28]. Geometry optimization was carried out using the B3LYP/6-31G (d) functional and basis set. All calculations were performed in the gas phase. Single point calculations for HOMO (Highest Occupied Molecular Orbital) and LUMO (Lowest Unoccupied Molecular Orbital) were determined at ground state (S₀) and first excited state (S₁) from optimized geometries. The electron density and spatial orientation of the HOMO and LUMO, and electrostatic potential maps (ESP) [29] were obtained using the same function. Electronic transitions were calculated using ZINDO method and STO-6G basis set in ArgusLab software from optimized geometry by B3LYP/6-31G (d) in Gaussian 03. To visualize the results, the Gauss view 5 software was used.

3. Results and discussion

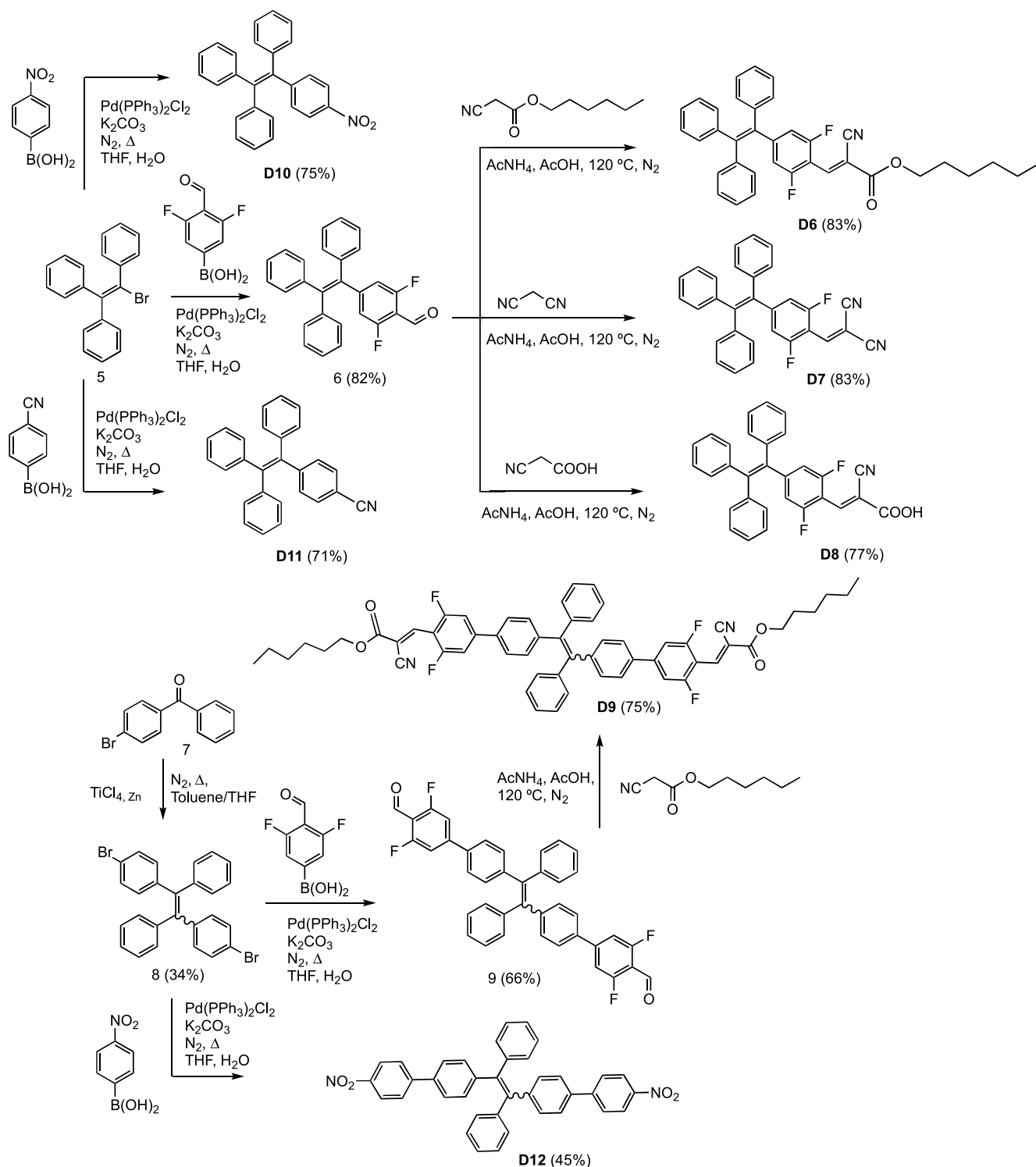
3.1. Synthesis of TPE derivatives

Here we report the design, synthesis and characterization of new luminescent TPE derivatives (Scheme 1) comprising TPE moiety as a donating group linked to (1) one of the following electron acceptors: nitro, cyano, dicyano, cyanoacetic acid, hexyl cyanoacetate, (TPE-A) or (2) linked to two electron acceptors: nitro or hexyl cyanoacetate, through a phenyl or di-fluorophenyl bridge (A- π -TPE- π -A), respectively.

The new luminescent materials with a TPE-A (D6-8, 10–11) and A- π -TPE- π -A (D9, D12) molecular structure were synthesized in moderate to high yields (45–83%) using the Suzuki coupling reaction and Knoevenagel condensation. The synthetic routes are presented in Scheme 2 and the detailed synthetic procedures are described in the Experimental Section. All synthesized derivatives were structurally characterized by ¹H and ¹³C NMR spectroscopy, FTIR, and mass spectrometry (see the Experimental Section for more details. The spectral data are consistent with the proposed structures.

3.2. Photophysical properties

The photophysical properties of TPE derivatives D6-D12 were studied in 1,4-dioxane solution and in Zeonex film. Fig. 1 shows the normalized absorption and emission spectra and the relevant spectroscopic data are summarized in Table 1. The absorption spectra of the TPE derivatives in 1,4-dioxane (Fig. 1A) are quite different, with a strong absorption band at around 250–300 nm, and a low to high intensity band around 325–400 nm depending on the acceptor group linked to the TPE core. The band at the higher wavelength is attributed to ICT from electron donor to electron acceptor group, whilst the lowest wavelength band is due to π - π^* transition from TPE core and depends on the conjugated π -system of the molecule [30]. The derivatives D11 (cyano) and D12 (di-NO₂) show intensive ICT absorption bands with the maximum wavelength (λ_{\max}) at 355 nm and 323 nm, respectively. The molar absorption coefficients (ϵ_{\max}) for all derivatives ranged between 8394 and 37,809 M⁻¹ cm⁻¹ at the absorption maximum (Table 1). Derivatives D9 and D12 with two acceptor groups in their molecular structure (A- π -TPE- π -A), show the higher ϵ_{\max} values, 37,809 and 22,498 M⁻¹ cm⁻¹, respectively, which could be due to their greater conjugated π -system. Specifically, for the di-substituted TPE D9, ϵ_{\max} value is 3 times greater than the correspondent mono-substituted derivative D6 and a slight redshift of 9 nm is observed. It is also noteworthy that the introduction of a hexyl chain in cyanoacetic acid group of D8, reduce the



Scheme 2. Synthetic routes and molecular structures of TPE derivatives D6-D12.

ϵ_{max} value from 12,237 to 8394 M⁻¹cm⁻¹ causing a redshift of 14 nm. The solution photoluminescence (PL) spectra of D6-D12 derivatives (Fig. 1B) show a maximum emission band (λ_{em}) between 401 and 547 nm. In the case of D6, D7, D8, D10, and D11, a shoulder is also observed around 502, 425, 497, 415, 483 nm, respectively, that disappears in the Zeonex film PL emission spectra (Fig. 1C). We attribute this observation to an excited-state rotamer with weak ICT formed in solution which disappears in solid state, due to the suppression of excited state intramolecular rotation of bulky groups in a rigid medium [31]. In the case of

the di-substituted TPE derivatives D9 and D12, a unique emission band is observed, at 362 nm and 345 nm, respectively, since the existence of rotamers in solution is restricted due to their large chemical structures. The Stokes shifts of the compounds in solution, range between 68 and 184 nm and reflect the feature of ICT that is intrinsically associated with the fluorophores [40]. Fluorescence quantum yields (ϕ_{F}) of D6-D12 in 1, 4-dioxane solution, were determined by comparative method using coumarin 153 in ethanol as fluorescence standard (ϕ_{F} 32%), and the obtained values range from 0.05 to 0.73%. These results are consistent

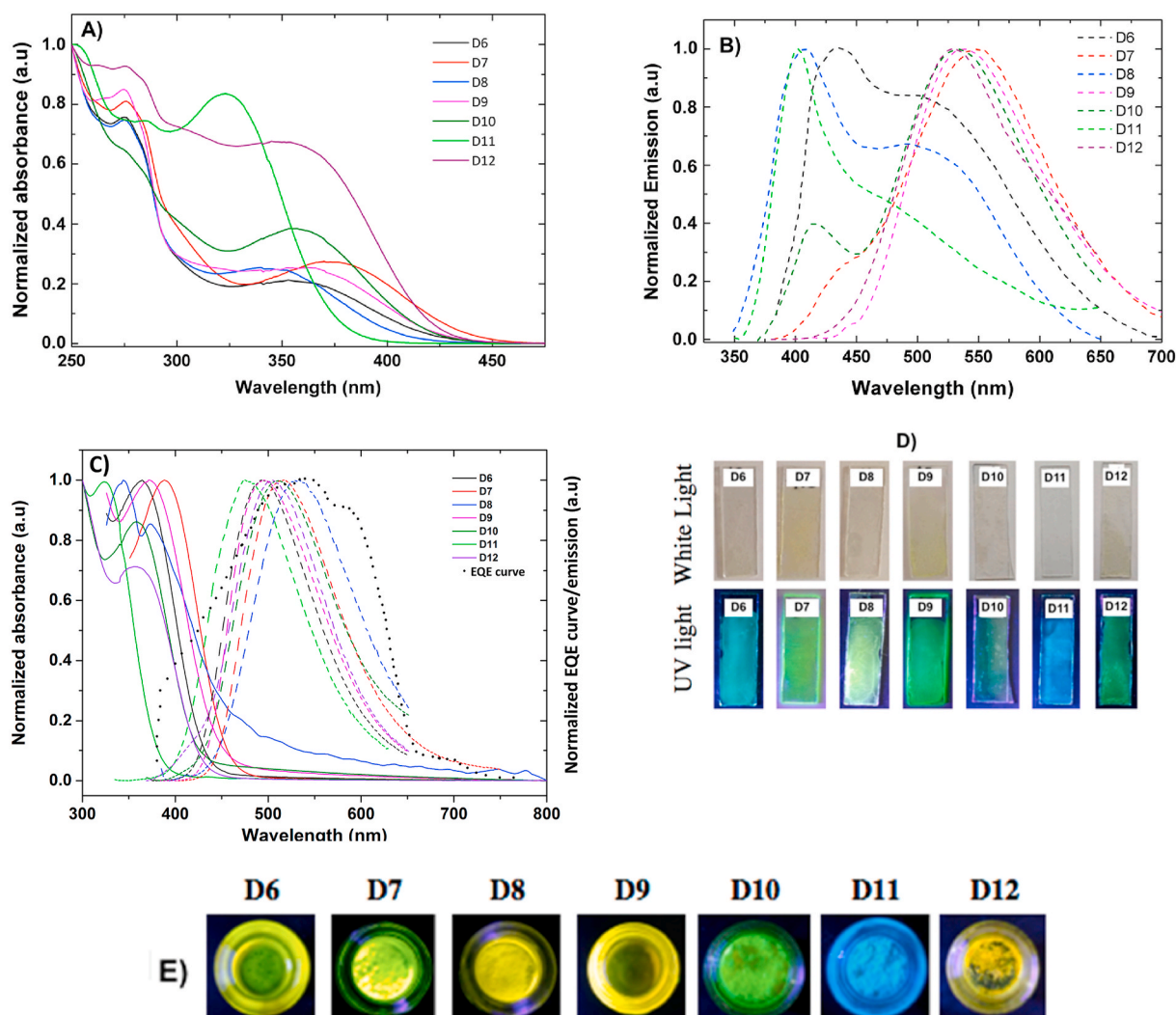


Fig. 1. Normalized absorption (solid line) (A), fluorescence emission (dashed line) (B) spectra of D6-D12 in 1,4-dioxane and Zeonex film (C). The normalized External Quantum Efficiency (EQE) curve of P3HT:PCBM solar cell [17] is shown as black dotted line (C). Images of Zeonex films based on D6-D12 derivatives under white and ultraviolet light of 365 nm (D), and TPE derivatives powders under ultraviolet light of 365 nm (E).

Table 1

Photophysical properties of TPE derivatives in 1,4-dioxane (experimental and theoretical) and Zeonex films.

	UV-Vis absorption λ_{\max} (nm)			Fluorescence emission ^b λ_{\max} (nm)		Stokes shift λ (nm)	
	1,4-dioxane	Film	Theoretical	1,4-dioxane	Film	1,4-dioxane	Film
D6	353 (8394) ^a	364	378	435 (0.36) ^c	494	82	130
D7	371 (11,473)	388	392	547 (0.14)	515	176	127
D8	339 (12,267)	344	379	407 (0.05)	531	68	187
D9	362 (37,809)	372	353	538 (0.73)	495	176	123
D10	355 (11,633)	359	413	532 (0.07)	512	177	153
D11	323 (12,928)	323	331	401 (<LOD) ^d	476	78	153
D12	345 (22,498)	357	359	529 (0.13)	505	184	148

^a Experimental molar absorption coefficient in $M^{-1} cm^{-1}$ in parenthesis.

^b The λ_{\max} abs of each derivatives was used as excitation wavelength.

^c Photoluminescence Quantum yield (%) in parenthesis. Coumarin 153 (38%) in ethanol with excitation at 420 nm was used as fluorescence standard.

^d LOD – Limit Of Detection.

with the visually observed low fluorescent of D6-D12 in solutions. In the case of D11 it was not possible to measure ϕ_F , because the fluorescence signal intensity is below the Limit of detection (LOD). Fig. 1 (D and E) shows the images of synthesized TPE derivatives in solid state under ultraviolet light of 365 nm, where an intense fluorescence emission of blue, green and yellow colors can be seen. The low ϕ_F of D6-D12 in solution and the high fluorescence visually observed in solid state point

out to the AEE characteristic already observed in other TPE derivatives [32,33], which is caused by the inhibition of intramolecular rotation in the single molecule state.

The photophysical properties of D6-D12 were also studied in films, using Zeonex polymer, which has good optical transparency in the near UV range [34]. Fig. 1C depicts the absorption and emission spectra of D6-D12 in films. As shown, there is no significant difference in the λ_{\max}

of TPE derivatives in both solution and films spectra. In fact only a redshift of approximately 10 nm is observed between their 1,4-dioxane solution and Zeonex solid samples. It is well known by the Franck-Condon principle [35] that the electron transition speed is extremely faster (femtoseconds) than the process of molecular relaxation. Consequently, the absorption process is less environmentally dependent which can explain the little difference between the λ_{max} of D6-D12 in solution and films. On the other hand, the emission process is more environmentally dependent and the shape and the maximum wavelength of the emission bands (λ_{em}) changed considerably in film spectra.

In this case, only a single emission band in the range 476–531 nm is observed for all derivatives. As shown in Fig. S1, the aforementioned shoulder observed in PL solution spectra of D6, D8 and D11, attributed to the low energy ICT emitting conformer, becomes dominant in film spectra with an emission maximum at 494, 531 and 476 nm, respectively. As expected the observed redshift in the λ_{em} leads to an increase of Stokes shift. In the case of D7, D9, D10 and D12 films a blue shift between 20 and 43 nm is observed in the single emission band, leading to a decrease in Stokes shift values. Nevertheless, in Zeonex films all derivatives show large Stokes shift between 123 and 187 nm, which will allow to minimize self-absorption losses in LDS application.

Luminescent polymethylmethacrylate (PMMA) films were prepared by spin coating technique from polymer solution doped with different concentrations of the TPE derivatives D8 and D11. These were chosen because they present its maximum absorption in the UVA part of the spectrum (310–410 nm range) having also the highest Stokes shift values, 187 and 153 nm, respectively (Fig. S2). The polymer solution was doped by different dye concentrations ranging from 0.03 to 0.57 wt %, and PL emission spectra of LDS films are shown in Fig. 2 and Fig. S4, in the wavelength range of 400–700 nm. Excitation wavelength of 370 and 380 nm were used for D8 and D11, respectively. A plot of the maximum fluorescence intensity as a function of the dye concentration is shown in Fig. 2 (inset).

The spectra show a remarkable dependence on the dye concentration since the fluorescence intensity increases with increasing concentration up to 0.34 wt %. For higher concentrations, the emission intensity starts to decrease, and in the case of D8 a redshift of 25 nm in λ_{em} is also observed. This may be explained by the fact that in a higher concentration range, the non-planar molecules, D8 and D11, become more closely packed and consequently the intermolecular π - π stacking interactions are enhanced, which promotes the formation of aggregates with ordered or random structures. With the increase of this competing force in the luminogen system, the AEE gives rise to fluorescence Aggregation-Caused Quenching (ACQ), which is responsible for the observed decreasing of fluorescence emission. In the case of D8, the

redshift of 25 nm observed in the λ_{em} may be due to the presence of the carboxylic group that facilitate the intermolecular interaction and hydrogen bonds, leading to the formation of J-aggregates, which are side-by-side molecular arrangements that cause bathochromic shift in the absorption and emission spectra [36–38]. On the other hand, the absorbance of films (Fig. S3) increased by increasing the concentration of the dye over the entire concentration range tested. The absorption and emission spectra of D8-and D11-LDS films obtained with five different dye concentrations (0.03, 0.06, 0.11, 0.34 and 0.57 wt%), showed that the higher absorption and fluorescence intensity were achieved for films containing 0.34 wt% of D8 and D11.

3.3. Thermal analysis

The melting points of the D7, D10 and D11 range from 148 to 173 °C. D6 and D9 with the hexylcyanoacetate acceptor group in the molecular structure, are viscous oils. The derivative D8 and D12 show higher melting point, which are 224–226 °C and 254–256 °C, respectively.

Thermal stability of the TPE derivatives was evaluated by TGA analysis and TGA (A) and dTGA (B) thermograms are shown in Fig. 3. All derivatives exhibited initial mass loss at temperature above 225 °C. For derivatives D9, a mass loss of 18% occurred between 125 and 250 °C (Fig. S5), possibly due to the evaporation of the solvent trapped inside. In the case of D7, D10 and D11 the mass loss occur between 225 and 400 °C and the estimated temperature at which the degradation rate is maximum (Tp, the peak temperature of the DTGA curve- Fig. 3b), is Tp 343, 351 and 347 °C, respectively.

The derivatives D6 and D12 are thermally more stable than the other ones, with the mass loss occurring between 250 and 550 °C, and Tp of 391 and 410 °C, respectively. The TGA results suggest that the type of acceptor substituents affects the thermal properties of synthesized TPE derivatives. Knowing that operating temperature of PV panels can get as hot as 65 °C, we conclude that all compounds (D6-D12) have good thermal stability for use in LDS layer.

3.4. Electrochemical properties

The electrochemical properties of D6-D12 were determined by cyclic voltammetry in freshly distilled acetonitrile solution using 0.1 M of tetrabutylammonium hexafluorophosphate (TBAPF6) as supporting electrolyte (Fig. 4). The potential was externally calibrated by ferrocene/ferrocenium couple (Fc/Fc⁺) and then was calculated versus NHE electrode. Cyclic voltammograms of D6, D9, D10 and D11 show quasi-reversible waves with two oxidation peaks between 1 and 1.5 eV whereas in derivatives D7, D8 and D12 the oxidation process is irreversible. The HOMO levels were estimated from the first oxidation onset

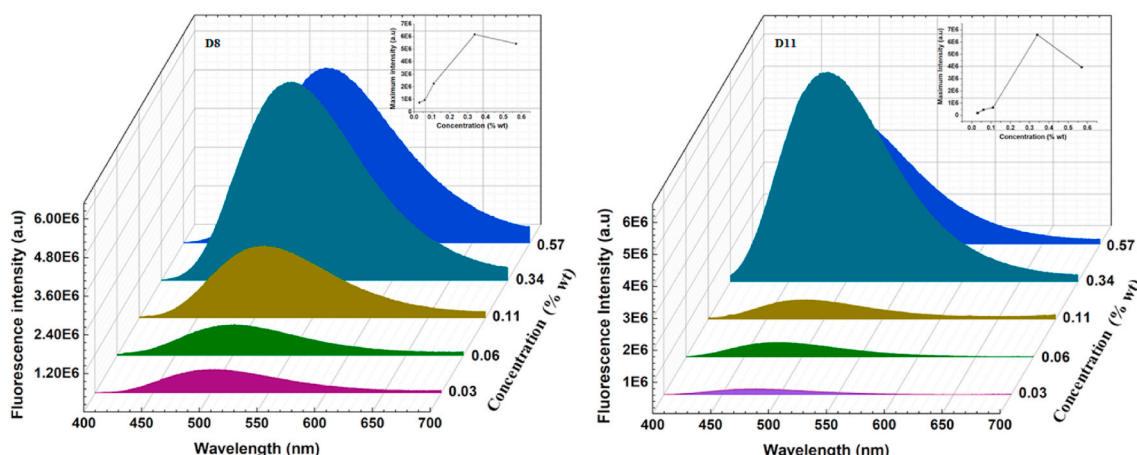


Fig. 2. Effect of concentration of the dyes D8 and D11 on the fluorescence emission of the LDS film.

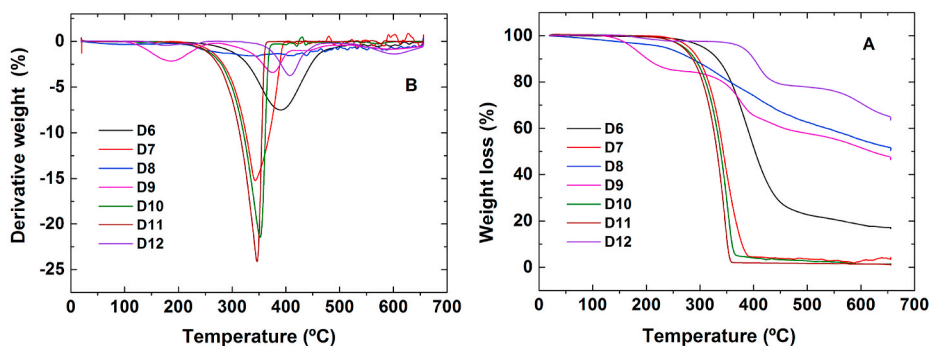


Fig. 3. Thermogravimetric (A) and derivative thermogravimetric (B) curves of synthesized TPE derivatives under nitrogen atmosphere at a heating rate of $10\text{ }^{\circ}\text{C min}^{-1}$.

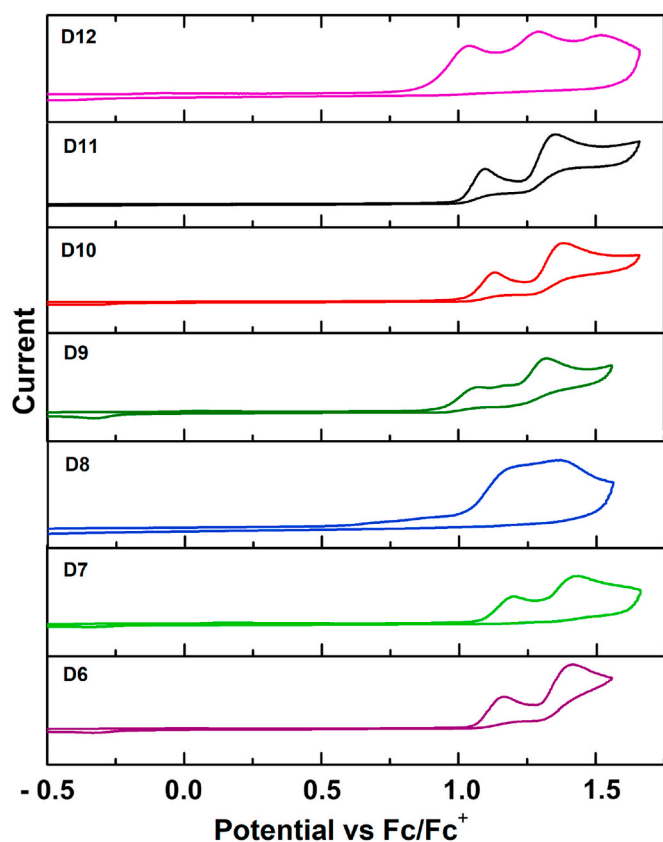


Fig. 4. Cyclic voltammograms of TPE derivatives in acetonitrile with TBAPF6 (0.1 M) as the electrolyte; scan rate: 50 mV/s. All voltammograms were referenced to internal ferrocene (Fc/Fc^+).

wave ($E_{\text{ox}}^{\text{onset}}$) by using the empirical equation ($E_{\text{HOMO}} = -(E_{\text{ox}}^{\text{onset}} + 4.8)$) [39]. The energy gap values (E_{0-0}) were estimated from the intercept of the normalized absorption and emission spectra in film.

The LUMO levels were determined by equation ($E_{\text{LUMO}} = E_{\text{HOMO}} + E_{0-0}$). Electrochemical properties are present in Table 2. The energy gap determined by cyclic voltammetry measurement for these new derivatives (2.76–3.15 eV) is similar to the energy gap reported in the literature (2.75–3.11 eV) for other TPE derivatives [27]. However, it is noticeable that the substituents on the TPE units affect the HOMO and LUMO energy levels of the TPE derivatives.

3.5. Quantum chemical calculations

Theoretical calculations were performed with Density Functional

Table 2

Electrochemical properties of TPE derivatives determined by cyclic voltammetry and DFT method.

TPE	$E_{\text{ox}}^{\text{onset}}$ vs Fc/Fc^+	$\lambda_{\text{int}}^{\text{a}}$ (nm)	E_{0-0}^{b} (eV)	Experimental (CV)		Theoretical (DFT)	
				E HOMO ^c (eV)	E LUMO ^d (eV)	E HOMO ^e (eV)	E LUMO ^e (eV)
D6	0.95	429	2.89	-5.75	-2.86	-5.74	-2.45
D7	1.08	450	2.76	-5.88	-3.12	-5.9	-2.86
D8	0.99	459	2.7	-5.79	-3.09	-5.80	-2.56
D9	1.07	440	2.81	-5.87	-3.06	-5.71	-2.64
D10	1.04	429	2.89	-5.84	-2.95	-5.61	-2.56
D11	1.02	394	3.15	-5.82	-2.67	-5.9	-2.01
D12	0.88	419	2.96	-5.68	-2.72	-5.71	-2.56

^a The intersect of the normalized absorption and the emission spectra in solid films.

^b E_{0-0} values were estimated from the intercept of the normalized absorption and emission spectra.

^c Deduced from equation $E_{\text{HOMO}} = -(E_{\text{ox}}^{\text{onset}} + 4.8)$.

^d Deduced from equation $E_{\text{LUMO}} = E_{\text{HOMO}} + E_{0-0}$.

^e Calculated with B3LYP/6-31G(d) in gaussian 03.

Theory (DFT) using Gaussian 03 software package [28] in order to better understand the photophysical properties of synthesized TPE derivatives.

The calculated transitions associated with their oscillator strengths, excitation energies and configuration interaction (CI) coefficients, as well as experimental wavelengths for comparison purpose are shown in Table S1. The calculation results allowed to observe that the transition of greater wavelength occurred between HOMO and LUMO. A good correlation is observed between the experimental and theoretical absorption maxima in 1,4-dioxane with small to moderate variation of 24, 21, 40, 9, 58, 6 and 14 nm for D6, D7, D8, D9, D10, D11 and D12, respectively. If compared with experimental absorption spectra data in Zeonex films, the difference is smaller (14, 4, 35, 19, 54, 8 and 2 nm for D6, D7, D8, D9, D10, D11 and D12, respectively).

The geometry structures of the TPE derivatives were optimized at the B3LYP/6-31G (d) level [40,41] and the electron density distribution for the HOMO and LUMO orbitals and its corresponding energy levels were subsequently calculated (Fig. 5). For all TPE derivatives, the HOMO orbital is located predominantly on the TPE core and has a greater contribution from the p_z orbital. On the other hand, the LUMO orbital is located on the substituted acceptor moiety, except for D11, where it is uniformly distributed throughout the molecular structure due to the weak acceptor character of the cyano group. In general, HOMO is located orthogonal to the plane of the molecule and it is a bonding molecular orbital (π), while LUMO is also orthogonal to the plane of the molecule, but as a non-bonding molecular orbital (π^*).

The results of theoretical studies also evidenced the presence of both $\pi-\pi^*$ and ICT transition for D6-D12, although, the contribution of one transition can be greater depending on the nature of the electrons donor

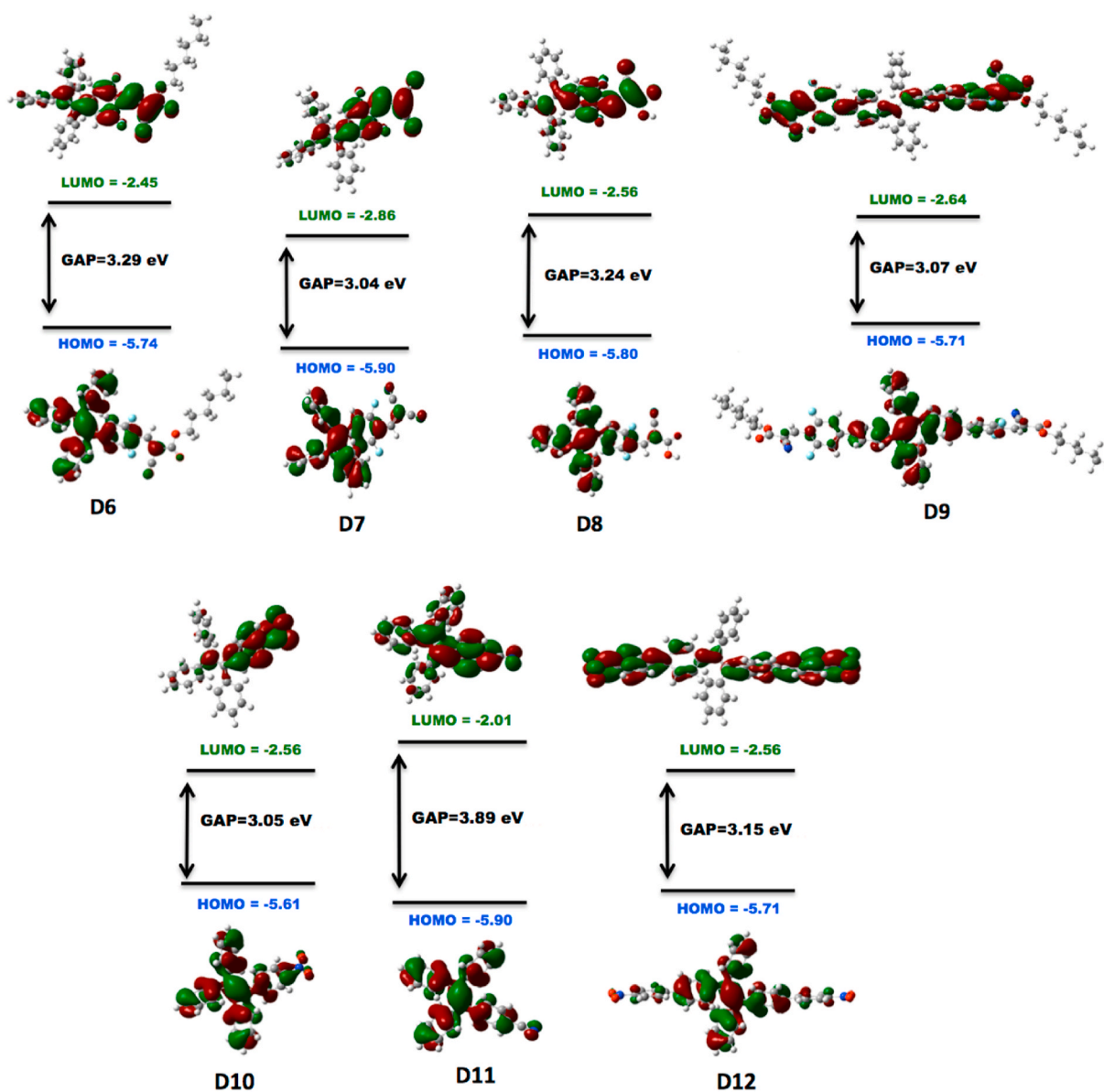


Fig. 5. Electron density distributions of HOMO and LUMO orbitals and corresponding energy levels (isovalue = 0.02 au).

and acceptor [42,43]. For example, as shown in Fig. 5, the well separated electronic distributions in the HOMO and LUMO orbitals at two different ends featuring donor and acceptor characters for all derivatives, except for D11, is expected to produce a charge-transfer between HOMO and LUMO [44]. The weak charge separation observed between the TPE core and the cyano group in D11 was also reflected in its experimental absorption spectrum, where a considerable difference in wavelength was observed in relation to other derivatives due to the electron-withdrawing strength of the acceptor group. The electrostatic potential maps (ESP) were also determined by TDF method and are shown in Fig. S6.

The estimated energy levels of HOMO and LUMO orbitals as well as the energies gap determined by theoretical calculations are consistent with those determined by cyclic voltammetry (CV) measurement (Table 2). The calculated energies gap between frontiers orbitals by DFT ranged from 3.04 to 3.89 eV, and are also in accordance with the gap energies reported in the literature (2.94–3.48 eV) [27] for other TPE derivatives, using the same functional and basis set (B3LYP/6-31G).

4. Conclusion

In this paper, we have successfully synthesized a series of TPE LDS compounds, presenting in their TPE-A or A- π -TPE- π -A molecular structure, groups (A) with different electron withdrawing strength. The results of the quantum chemical studies are consistent with experimental results, evidencing the existence of ICT between donor and acceptor moieties through the analysis of the electron density of frontier orbitals. All compounds present high absorption in the UV region (from 323 nm to 388 nm) and fluorescence emission band close to the region of higher external quantum yield of organic solar cells (476–531 nm). The large Stokes shift found in all compounds (from 123 up to 187 nm), will allow to minimize self-absorption losses in LDS layer application. All derivatives exhibited high thermal stability with the decomposition temperature above 225 °C. In compounds D6 and D9, the presence of the hexyl chain in the cyanoacetate group has impact on their physical state, i.e. these are highly viscous oil instead of solids. The preliminary studies on D8- and D11-based LDS layers (TPE derivatives with larger stoke shift, 187 and 153 nm, respectively) prepared at different dye concentrations, points out to 0.34 wt% of dye-doped PMMA films, in which high

filtration of UV radiation and emission intensity is achieved simultaneously.

The performance of these D6-D12 based LDS layers in organic photovoltaic cells is underway and will be reported in due course. It is expected to increase the cell's lifetime by blocking the UV radiation, while preserving an excellent light transmission across the visible spectrum.

CRedit authorship contribution statement

Hélio Lopes Barros: Investigation, Writing – original draft, Visualization, Data curation. **Maria Alexandra Esteves:** Investigation, Writing – review & editing, Data curation. **Maria João Brites:** Conceptualization, Investigation, Writing – review & editing, Resources, Supervision.

Declaration of competing interest

The authors declare that they have no known competing financial interests or personal relationships that could have appeared to influence the work reported in this paper.

Acknowledgments

This work was supported by Horizon H2020/European Commission under the Project IDEAS (Novel building Integration Designs for increased Efficiencies in Advanced climatically tunable renewable energy Systems) Grant agreement ID: 815271. H. Barros was supported by a postdoctoral grant from the same project.

Appendix A. Supplementary data

Supplementary data to this article can be found online at <https://doi.org/10.1016/j.dyepig.2021.109724>.

References

- [1] Kettle J, Bristow N, Gethin DT, Tehrani ZT, Moudam O, Li B, et al. Printable luminescent down shifter for enhancing efficiency and stability of organic photovoltaics. *Sol Energy Mater Sol Cells* 2016;144:481–7. <https://doi.org/10.1016/j.solmat.2015.09.037>.
- [2] Hsu HL, Chen CP, Chang JY, Yu YY, Shen YK. Two-step thermal annealing improves the morphology of spin-coated films for highly efficient perovskite hybrid photovoltaics. *Nanoscale* 2014;6:10281–8. <https://doi.org/10.1039/c4nr02751e>.
- [3] Benfadel K, Kaci S, Hamidouche F, Keffous A, Benmounah A, Manseri A, et al. Development of an antireflection layer using a LDS based on β -SiC nanoparticles. *Siliconindia* 2020;1–13. <https://doi.org/10.1007/s12633-020-00551-w>.
- [4] Klampafits E, Ross D, McIntosh KR, Richards BS. Enhancing the performance of solar cells via luminescent down-shifting of the incident spectrum: a review. *Sol Energy Mater Sol Cells* 2009;93:1182–94. <https://doi.org/10.1016/j.solmat.2009.02.020>.
- [5] Li Y, Li Z, Ablekim T, Ren T, Dong WJ. Rational design of tetraphenylethylene-based luminescent down-shifting molecules: photophysical studies and photovoltaic applications in a CdTe solar cell from small to large units. *Phys Chem Chem Phys* 2014;16:26193–202. <https://doi.org/10.1039/c4cp03521f>.
- [6] Uddin A, Upama M, Yi H, Duan L. Encapsulation of organic and perovskite solar cells: a review. *Coatings* 2019;9:65. <https://doi.org/10.3390/coatings9020065>.
- [7] Fernandes RV, Bristow N, Stoichkov V, Anzelli HS, Duarte JL, Laureto E, et al. Development of multidyed UV filters for OPVs using luminescent materials - IOPscience. *J Phys D Appl Phys* 2017;50:025103.
- [8] Roth B, Dos Reis Benatto GA, Corazza M, Sondergaard RR, Gevorgyan SA, Jørgensen M, et al. The critical choice of PEDOT:PSS additives for long term stability of roll-to-roll processed OPVs. *Adv Energy Mater* 2015;5. <https://doi.org/10.1002/aenm.201401912>.
- [9] Abdel-Fattah TM, Younes EM, Namkoong G, El-Maghraby EM, Elsayed AH, Abo Elazm AH. Stability study of low and high band gap polymer and air stability of PTB7:PC71BM bulk heterojunction organic photovoltaic cells with encapsulation technique. *Synth Met* 2015;209:348–54. <https://doi.org/10.1016/j.synthmet.2015.08.005>.
- [10] Weerasinghe HC, Rolston N, Vak D, Scully AD, Dauskardt RH. A stability study of roll-to-roll processed organic photovoltaic modules containing a polymeric electron-selective layer. *Sol Energy Mater Sol Cells* 2016;152:133–40. <https://doi.org/10.1016/j.solmat.2016.03.034>.
- [11] Fernandes RV, Urbano A, Duarte JL, Bristow N, Kettle J, Laureto E. Tuning the optical properties of luminescent down shifting layers based on organic dyes to increase the efficiency and lifetime of P3HT: PCBM photovoltaic devices. *J Lumin* 2018;203:165–71. <https://doi.org/10.1016/j.jlumin.2018.06.053>.
- [12] Cheng Z, Su F, Pan L, Cao M, Sun Z. CdS quantum dot-embedded silica film as luminescent down-shifting layer for crystalline Si solar cells. *J Alloys Compd* 2010;494:L7. <https://doi.org/10.1016/j.jallcom.2010.01.047>.
- [13] Meng L, Wu XG, Ma S, Shi L, Zhang M, Wang L, et al. Improving the efficiency of silicon solar cells using in situ fabricated perovskite quantum dots as luminescence downshifting materials. *Nanophotonics* 2020;9:93–100. <https://doi.org/10.1515/nanoph-2019-0320>.
- [14] Singh P, Shahi PK, Singh SK, Singh AK, Singh MK, Prakash R, et al. Lanthanide doped ultrafine hybrid nanostructures: multicolour luminescence, upconversion based energy transfer and luminescent solar collector applications. *Nanoscale* 2017;9:696–705. <https://doi.org/10.1039/c6nr07250j>.
- [15] Van Der Ende BM, Aarts L, Meijerink A. Lanthanide ions as spectral converters for solar cells. *Phys Chem Chem Phys* 2009;11:11081–95. <https://doi.org/10.1039/b913877c>.
- [16] Ahmed H, Sethi A, Doran J, McCormack SJ. Plasmonic interaction in enhanced luminescent down-shifting layers for photovoltaic devices. *Nova Science Publishers, Inc Plasmon. Adv. Res. Appl* 2016:1–68.
- [17] Pardo Perdomo A, Vignoto Fernandes R, Artico Cordeiro NJ, Franchello F, Toledo Da Silva MA, Leonil Duarte J, et al. Luminescent down-shifting film based on optimized mixture of organic dyes for improving the performance of P 3 HT: PC 61BM photovoltaic devices. *J Appl Phys* 2020;128:035502. <https://doi.org/10.1063/5.0003629>.
- [18] BASF AG. Collector dyes technical Information Lumogen F Colorants and Graphic systems. 1997.
- [19] Zhao Z, Lam JWY, Tang BZ. Tetraphenylethene: a versatile AIE building block for the construction of efficient luminescent materials for organic light-emitting diodes. *J Mater Chem* 2012;22:23726–40. <https://doi.org/10.1039/c2jm31949g>.
- [20] Zhang F, Fan J, Yu H, Ke Z, Nie C, Kuang D, et al. Nonplanar organic sensitizers featuring a tetraphenylethene structure and double electron-withdrawing anchoring groups. *J Org Chem* 2015;80:9034–40. <https://doi.org/10.1021/acs.joc.5b01140>.
- [21] Li CT, Kuo YL, Kumar CP, Huang PT, Lin JT. Tetraphenylethylene tethered phenothiazine-based double-anchored sensitizers for high performance dye-sensitized solar cells. *J Mater Chem* 2019;7:23225–33. <https://doi.org/10.1039/c9ta09025h>.
- [22] Danos L, Parel T, Markvart T, Barrioz V, Brooks WSM, Irvine SJC. Increased efficiencies on CdTe solar cells via luminescence down-shifting with excitation energy transfer between dyes. *Sol Energy Mater Sol Cells* 2012;98:486–90. <https://doi.org/10.1016/j.solmat.2011.11.009>.
- [23] Williams DBG, Lawton M. Drying of organic solvents: quantitative evaluation of the efficiency of several desiccants. *J Org Chem* 2010;75:8351–4. <https://doi.org/10.1021/jo101589h>.
- [24] Nicolas J, Bensaïd F, Desmaële D, Grogna M, Detrembleur C, Andrieux K, et al. Synthesis of highly functionalized poly(alkyl cyanoacrylate) nanoparticles by means of click chemistry. *Macromolecules* 2008;41:8418–28. <https://doi.org/10.1021/ma8013349>.
- [25] Brandsma L, Verkrujse HD. Synthesis of acetylenes, allenes and cumulenes : methods and techniques. Elsevier; 2004.
- [26] Shafiee A, Yahaya M. Determination of HOMO and LUMO of [6,6]-Phenyl C61-butyric acid 3-ethylthiophene ester and poly (3-octyl-thiophene-2, 5-diyl) through voltametry characterization (Penentuan HOMO dan LUMO asid [6,6]-Fenil C61-butirik ester 3-etiltiofena dan Poli (3-oktil-tiofena-2, 5-diyl) menerusi Pencirian voltametri). *Sains Malays* 2011;40:173–6.
- [27] Feng X, Qi C, Feng HT, Zhao Z, Sung HHY, Williams ID, et al. Dual fluorescence of tetraphenylethylene-substituted pyrenes with aggregation-induced emission characteristics for white-light emission. *Chem Sci* 2018;9:5679–87. <https://doi.org/10.1039/c8sc01709c>.
- [28] Inc. GS-, Wallingford U, CT U Frish M, Trucks G, Schlegel H, et al. Gaussian 03, Revision D. 02. Pittsburgh PA: Gaussian Inc; 2003.
- [29] Gupta VP. Electron density analysis and electrostatic potential. *Princ. Appl. Quantum Chem. Elsevier*; 2016. p. 195–214. <https://doi.org/10.1016/b978-0-12-803478-1.00006-6>.
- [30] Baheti A, Lee CP, Thomas KRJ, Ho KC. Pyrene-based organic dyes with thiophene containing π -linkers for dye-sensitized solar cells: optical, electrochemical and theoretical investigations. *Phys Chem Chem Phys* 2011;13:17210–21. <https://doi.org/10.1039/c1cp21714c>.
- [31] Torres É, Berberan-Santos MN, Brites MJ. Synthesis, photophysical and electrochemical properties of perylene dyes. *Dyes Pigments* 2015;112:298–304. <https://doi.org/10.1016/j.dyepig.2014.07.019>.
- [32] Hou R, Zhao B, Xia Y, Li D. Organic fluorescent compounds that display efficient aggregation-induced emission enhancement and intramolecular charge transfer. *Molecules* 2018;23:1446. <https://doi.org/10.3390/molecules23061446>.
- [33] Peng HQ, Zheng X, Han T, Kwok RTK, Lam JWY, Huang X, et al. Dramatic differences in aggregation-induced emission and supramolecular Polymerizability of tetraphenylethene-based stereoisomers. *J Am Chem Soc* 2017;139:10150–6. <https://doi.org/10.1021/jacs.7b05792>.
- [34] Nunes PS, Ohlsson PD, Ordeig O, Kutter JP. Cyclic olefin polymers: emerging materials for lab-on-a-chip applications. *Microfluid Nanofluidics* 2010;9:145–61. <https://doi.org/10.1007/s10404-010-0605-4>.
- [35] Lakowicz JR. Principles of fluorescence spectroscopy. Springer Verlag; 2016.
- [36] El-Bashir S, AlSalhi M, Al-Faifi F, Alenazi W. Spectral properties of PMMA films doped by perylene dyestuffs for Photosensitive greenhouse cladding applications. *Polymers* 2019;11:494. <https://doi.org/10.3390/polym11030494>.

- [37] Rodrigues ACB, Seixas de Melo JS. Aggregation-induced emission: from small molecules to polymers—historical background, mechanisms and Photophysics. *Top Curr Chem* 2021;379. <https://doi.org/10.1007/s41061-021-00327-9>.
- [38] Yamaguchi M, Ito S, Hirose A, Tanaka K, Chujo Y. Control of aggregation-induced emission: versus fluorescence aggregation-caused quenching by bond existence at a single site in boron pyridinoiminate complexes. *Mater Chem Front* 2017;1:1573–9. <https://doi.org/10.1039/c7qm00076f>.
- [39] Pommerehne J, Vestweber H, Guss W, Mahrt RF, Bässler H, Porsch M, et al. Efficient two layer leds on a polymer blend basis. *Adv Mater* 1995;7:551–4. <https://doi.org/10.1002/adma.19950070608>.
- [40] Becke AD. Density-functional thermochemistry. III. The role of exact exchange. *J Chem Phys* 1993;98:5648–52. <https://doi.org/10.1063/1.464913>.
- [41] Lee C, Yang W, Parr RG. Development of the Colle-Salvetti correlation-energy formula into a functional of the electron density. *Phys Rev B* 1988;37:785–9. <https://doi.org/10.1103/PhysRevB.37.785>.
- [42] Sinha HK, Dogra SK. Ground and excited state prototropic reactions in 2-(*o*-hydroxyphenyl)benzimidazole. *Chem Phys* 1986;102:337–47. [https://doi.org/10.1016/0301-0104\(86\)80006-4](https://doi.org/10.1016/0301-0104(86)80006-4).
- [43] Roohi H, Hejazi F, Mohtamedifar N, Jahantab M. Excited state intramolecular proton transfer (ESIPT) in 2-(2'-hydroxyphenyl)benzoxazole and its naphthalene-fused analogs: a TD-DFT quantum chemical study. *Spectrochim Acta Part A Mol Biomol Spectrosc* 2014;118:228–38. <https://doi.org/10.1016/j.saa.2013.08.068>.
- [44] Hao X, Liang M, Cheng X, Pian X, Sun Z, Xue S. Organic dyes incorporating the Benzo[1,2-*b*:4,5-*b'*]dithiophene moiety for efficient dye-sensitized solar cells. *Org Lett* 2011;13:5424–7. <https://doi.org/10.1021/ol201858b>.